Volume 1, Number 4

JPCR | JOURNAL OF PEDIATRIC CASE REPORTS

A MULTIDISCIPLINARY JOURNAL OF CASE REPORTS

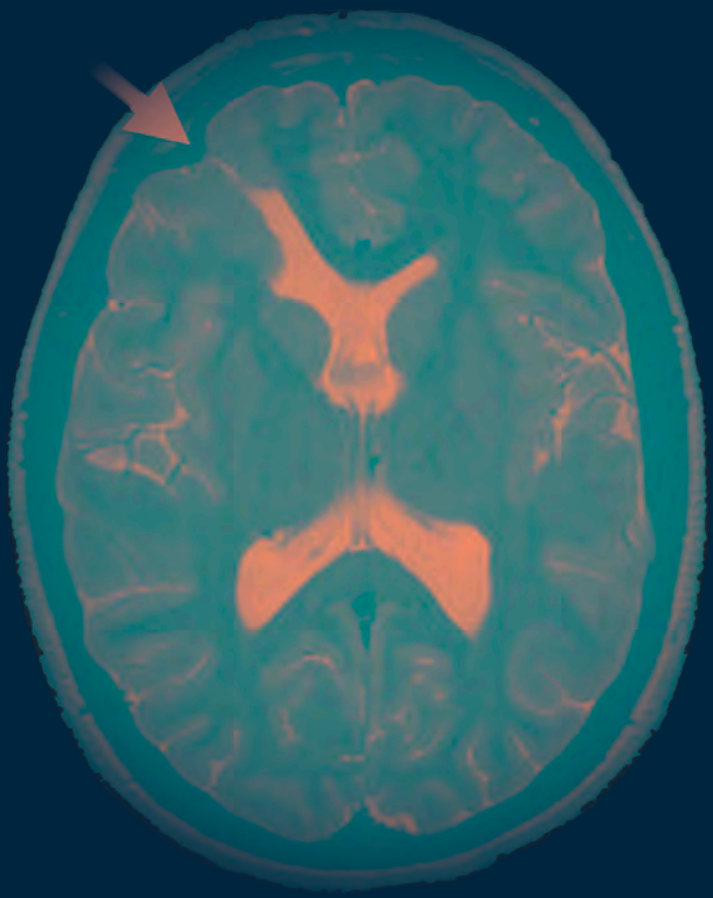

Double Outlet Right Ventricle

Stress Fractures in Children

Lymphangioleiomyomatosis

Schizencephaly

Double Aortic Arch Case

www.journalofpediatriccasereports.com

JPCR | JOURNAL OF PEDIATRIC CASE REPORTS

A MULTIDISCIPLINARY JOURNAL OF CASE REPORTS

Anderson Publishing, Ltd
180 Glenside Avenue,
Scotch Plains, NJ 07076
Tel: 908-271-8644

VOLUME 1 NUMBER 4

Double Outlet Right Ventricle

Ahmed Mohamed, BS; Richard B. Towbin, MD; Ranjit Philip, MD; Jason N. Johnson, MD,MHS; Alexander J. Towbin, MD

Abstract

Double outlet right ventricle (DORV) is characterized by an abnormal connection between both great arteries and the right ventricle, leading to poor systemic oxygenation. The diagnostic criteria for this condition vary, as do the various morphologies that exist. Echocardiography is the primary imaging tool, requiring views from multiple planes to elucidate the specific morphology of DORV in each patient, along with any associated cardiac anomalies. Incorporating other imaging modalities such as CT to maximize diagnostic accuracy is essential in determining the proper surgical approach, as the survival rate for children who undergo surgical repair remains high.

Keywords: cardiothoracic, cardiac, congenital

Case Summary

A 6-hour-old female presented with cyanosis and tachypnea with oxygen saturations in the 70s despite supplemental oxygen. On physical exam, the neonate was tachycardic with a hyperdynamic precordium, a soft systolic murmur, mild hepatomegaly, and decreased femoral pulses with delayed capillary refill. The transthoracic echocardiogram confirmed the diagnosis, and a chest CTA was performed for surgical planning.

Imaging Findings

Chest CTA with contrast (Figures 1, 2) showed a double outlet right ventricle (DORV) with malposition of the great arteries, subpulmonic ventricular septal defect (VSD), and aortic arch hypoplasia. This constellation of findings is often referred to as Taussig-Bing anomaly. The patient had an arterial switch operation, aortic arch augmentation, and VSD closure at 1 week of life. A repeat chest CTA (Figures 3, 4) at 2 years of age showed repair of the aortic arch with left pulmonary artery stenosis.

Diagnosis

Double outlet right ventricle.

As DORV can present similarly to and occur in conjunction with other congenital heart anomalies, the differential diagnoses include Tetralogy of Fallot, transposition of the great arteries and VSD.

Discussion

DORV is a congenital heart defect in which both great arteries (the aorta and the pulmonary artery) arise predominantly or entirely from the right ventricle instead of one from each ventricle. This can lead to symptoms of poor feeding, fatigue, clubbing, and cyanosis.[1] During normal fetal development, the heart's outflow tract initially originates from the right ventricle. The common outflow tract later divides and spirals to form the aorta and pulmonary artery, aligning one with the left ventricle and the other with the right ventricle. Endocardial cushions facilitate the development of the semilunar valves and the conal septum that separates the ventricular outflow tracks—an abnormality in this process can lead to DORV. Epidemiologic studies indicate that DORV occurs in anywhere between 3 and 24/100,000 live births, accounting for approximately 1-3% of all congenital heart defects.[1] Studies have been conducted to determine any genetic basis for the disease, with common associations seen with Trisomy 18, Trisomy 13, chromosome 8 abnormalities, and less commonly, in patients with 22q11 deletions. Associations with mutations in the *CFC1* and *CRX* genes have also been found.[1-3]

The guidelines for what level of right ventricular outflow is considered DORV versus what constitutes another congenital heart anomaly are debated. The 50% rule (also commonly referred to as the 150% rule) is often used to delineate DORV. The 50% rule states that a great artery is considered to arise from the right ventricle when over 50% of its circumference is connected to it.[1] However, measuring the level of association between the aorta and the right ventricle is impractical due to the lack of a definitive boundary and

Affiliations: University of Central Florida College of Medicine, Orlando, Florida (Mohamed); Department of Radiology, Phoenix Children's Hospital, Phoenix, Arizona (RB Towbin); Heart Institute, Le Bonheur Children's Hospital, Memphis, Tennessee (Philip, Johnson); Department of Radiology, Cincinnati Children's Hospital and University of Cincinnati College of Medicine, Cincinnati, Ohio (AJ Towbin).

Disclosures: The authors have no conflicts of interest to disclose. None of the authors received outside funding for the production of this original manuscript and no part of this article has been previously published elsewhere.

https://doi.org/10.37549/JPCR-26-0094

Figure 1. (A) Chest CTA with contrast in an axial plane at the ventricular mass. There is a large VSD in a patient with double outlet right ventricle (DORV). DA, descending aorta; LA, left atrium; LV, left ventricle; MV, mitral valve; RA, right atrium; RV, right ventricle; TV, tricuspid valve; VSD, ventricular septal defect. (B) Chest CTA with contrast in an axial plane at the pulmonary valve. The VSD is subpulmonic. DA, descending aorta; LA, left atrium; LAA, left atrial appendage; LUPV, left upper pulmonary vein; PV, pulmonary valve; RA, right atrium; RV, right ventricle; RUPV, right upper pulmonary vein. (C) Chest CTA with contrast in an axial plane at the aortic valve. The aortic valve arises from the right ventricle consistent with DORV. The main pulmonary artery is posterior to the aortic valve. AV, aortic valve; DA, descending aorta; LPA, left pulmonary artery; MPA, main pulmonary artery; RPA, right pulmonary artery; RV, right ventricle; RUPV, right upper pulmonary vein.

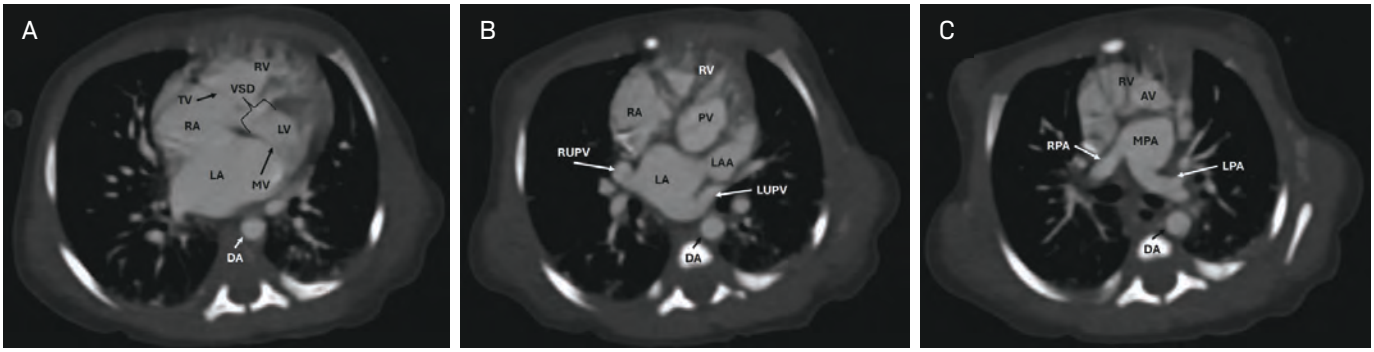

Figure 2. 3D chest CTA with contrast in a sagittal projection. The aorta is superior to the main pulmonary artery. The aortic arch is hypoplastic with coarctation. AA, ascending aorta; Coarct, coarctation; DA, descending aorta; Ductus, ductus arteriosus; IA, innominate artery; LCCA, left common carotid artery; LSA, left subclavian artery.

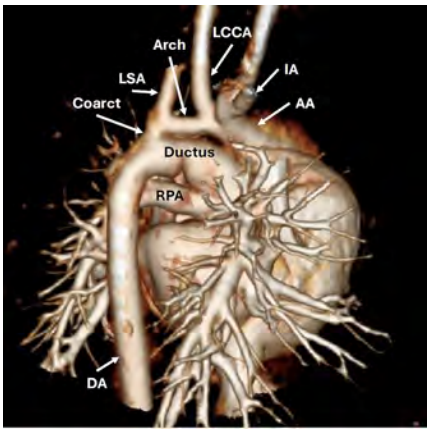

Figure 3. Chest CTA with contrast in an axial plane at the main pulmonary artery. The right pulmonary artery is anterior to the ascending aorta consistent with the arterial switch operation. AA, ascending aorta; DA, descending aorta; MPA, main pulmonary artery; RPA, right pulmonary artery; SVC, superior vena cava.

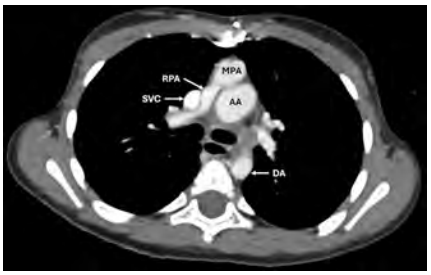

Figure 4. 3D chest CTA with contrast in a sagittal projection. The left pulmonary artery is anterior to the aorta and is stenotic. The aortic arch is normal in size. There is neo-aortic valve dilation. DA, descending aorta; LCCA, left common carotid artery; LPA, left pulmonary artery; LSA, left subclavian artery; MPA, main pulmonary artery; neo-AV, neo-aortic valve; neo-PV, neo-pulmonary valve.

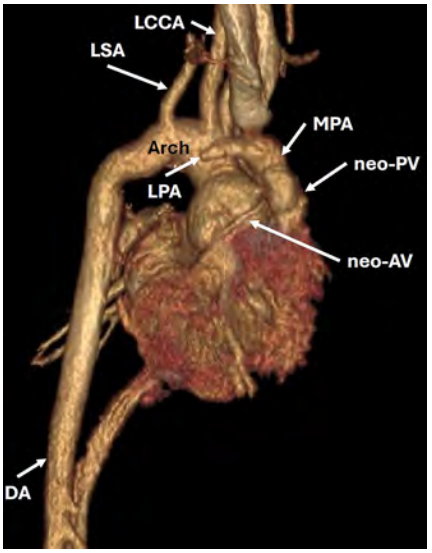

the difficulty in quantifying the three-dimensional nature of this junction using standard imaging.[4] DORV can occur with varying physiologies as the great arteries can be in different positions in relationship to the VSD. VSD is found in almost 100% of cases of DORV, with atrial septal defects occurring in approximately 10-30% of cases.[4,5] When DORV has a subaortic VSD, the physiology is like Tetralogy of Fallot, and when there is a subpulmonic VSD, the physiology is like transposition of the great arteries. DORV with a subpulmonary VSD is often associated with aortic arch hypoplasia and called Taussig-Bing anomaly.

DORV can present as an isolated defect or in combination with other congenital anomalies; recognizing these variations is essential for guiding surgical management.[5] Commonly, the right ventricle will have an infundibulum that supports both the aortic and pulmonary valves. In some cases, both a subaortic and subpulmonary infundibulum are present, which may coexist with an overriding aorta or, less commonly, an overriding pulmonary artery. While VSDs are present in nearly all cases of DORV, bilateral infundibula occur in only about 10-15% of cases, making their value as defining diagnostic features controversial.[6,7]

Many different imaging techniques can be used to diagnose DORV by determining whether both the pulmonary artery and the aorta primarily connect to the right ventricle. Echocardiography is most frequently used as an initial screening tool to differentiate the ventriculo-infundibular fold from the conal septum using views from different planes.[8] Commonly, the parasternal long-axis imaging plane is used to identify a lack of communication between the mitral valve and the aorta.[8] Cardiac catheterization can also be

performed but has largely been phased out due to its invasiveness and associated risks. MRI has also been used, with CT emerging more recently with improved spatial resolution and reduced acquisition times.[4] These imaging modalities are used to guide surgical strategies by uncovering the orientation of the great arteries, the conus, the presence and location of a VSD, and other associated cardiac anomalies.[9]

Treatment for DORV depends largely on the specific morphology, as a specific surgical approach is indicated depending upon the subtype of DORV. Surgical approaches are almost always biventricular, but univentricular repairs are sometimes required.[5] The most common approach used is the intraventricular tunnel (baffle) repair, where a patch is placed within the right ventricle to direct left ventricular outflow through the VSD to the aorta, thereby establishing physiological separation of the systemic and pulmonary circulations.[6] If the communication between the ventricles is subpulmonary, intraventricular baffling to the pulmonary trunk is performed, and an arterial switch operation is performed (moving the pulmonary artery anterior to the native aortic valve and moving the aorta posterior to the native pulmonary valve). The presence of other cardiac anomalies, such as pulmonary stenosis or aortic arch hypoplasia, may also impact the surgical approach and warrant further intervention. In cases where the VSD is noncommitted to the left ventricle or is subpulmonary and exhibits pulmonary stenosis, a double-root translocation procedure involving the relocation of both the pulmonary and aortic roots to restore normal directional flow is pursued.[6,10]

The most common complication that can occur is outflow obstruction to either of the ventricles, occurring in 3-30% of cases. Other postoperative complications include residual or recurrent VSDs, arrhythmias, and right ventricular dysfunction.[1] The long-term prognosis after successful surgical repair is generally favorable, with survival rates estimated between 80% and 95%.[2] Mortality is most attributed to progressive ventricular failure, severe arrhythmias, or obstruction of reconstructed outflow tracts, necessitating lifelong cardiac surveillance in these patients.[10]

Conclusion

DORV is characterized by an abnormal connection between both great arteries and the right ventricle leading to poor systemic oxygenation. The diagnostic criteria for this condition vary, as do the various morphologies that exist. Echocardiography is the primary imaging tool, requiring views from multiple planes to elucidate the specific morphology of DORV in each patient, along with any associated cardiac anomalies. Incorporating other imaging modalities such as CT to maximize diagnostic accuracy is essential in determining the proper surgical approach, as the survival rate for children who undergo surgical repair remains high.

References

1) Obler D, Juraszek AL, Smoot LB, Natowicz MR. Double outlet right ventricle: aetiologies and associations. *J Med Genet*. 2008;45(8):481-497. doi: 10.1136/jmg.2008.057984

2) Gedikbasi A, Oztarhan K, Gul A, Sargin A, Ceylan Y. Diagnosis and prognosis in double-outlet right ventricle. *Am J Perinatol*. 2008;25(7):427-434. doi:10.1055/s-0028-1083840

3) Goldmuntz E, Clark BJ, Mitchell LE, et al. Frequency of 22q11 deletions in patients with conotruncal defects. *J Am Coll Cardiol*. 1998;32(2):492-498. doi:10.1016/s0735-1097(98)00259-9

4) Kyriakopoulou V, Davidson A, Chew A, et al. Characterization of ASD traits among a cohort of children with isolated fetal ventriculomegaly. *Nat Commun Mar*. 2023;14:1550. doi:10.1038/s41467-023-3724209

5) Goo HW. Double outlet right ventricle: in-depth anatomic review using three-dimensional cardiac CT data. *Korean J Radiol*. 2021;22(11):1894-1908. doi:10.3348/kjr.2021.0248

6) Bell-Cheddar Y, Devine WA, Diaz-Castrillon C-E, et al. Double outlet right ventricle. *Front Pediatr*. 2023;11:1244558. doi:10.3389/fped.2023.1244558

7) Ebadi A, Spicer DE, Backer CL, Fricker FJ, Anderson RH. Double-outlet right ventricle revisited. *J Thorac Cardiovasc Surg*. 2017;154(2):598-604. doi:10.1016/j.jtcvs.2017.03.049

8) Mazzucco A, Faggian G, Stellin G, et al. Surgical management of double-outlet right ventricle. *J Thorac Cardiovasc Surg*. 1985;90(1):29-34.

9) Priya S, Nagpal P, Sharma A, Pandey NN, Jagia P. Imaging spectrum of double-outlet right ventricle on multislice computed tomography. *J Thorac Imaging*. 2019;34(5):W89-W99. doi:10.1097/RTI.0000000000000396

10) Mahle WT, Martinez R, Silverman N, Cohen MS, Anderson RH. Anatomy, echocardiography, and surgical approach to double outlet right ventricle. *Cardiol Young*. 2008;18(suppl 3):39-51. doi:10.1017/S1047951108003284

https://doi.org/10.37549/JPCR-26-0094

Stress Fractures in Children

Adrienne T. Ly, BA; Richard B. Towbin, MD; Carrie M. Schaefer, MD; Alexander J. Towbin, MD

Abstract

Stress fractures are microscopic disruptions of bone integrity that can occur in both children and adults. In pediatric patients, these injuries most commonly affect the lower extremities, particularly the tibia and metatarsals. Children involved in high-impact, running-intensive sports are at increased risk. Diagnosis can be challenging, as the microscopic nature of stress fractures makes them difficult to detect on radiographs. Advanced imaging modalities such as MRI and bone scintigraphy offer greater sensitivity for early detection. Because stress fractures typically do not result in displacement, treatment is generally conservative and includes activity modification, rest, and, in some cases, immobilization.

Keywords: musculoskeletal, lower extremity, trauma

Case Summary

An adolescent male high-jumper presented with worsening bilateral lower leg pain.

Imaging Findings

Initial radiograph of the left lower leg (Figure 1) was normal. MRI performed 5 days later (Figure 2) demonstrated edema-like signal in the medial proximal tibial metaphyses bilaterally. A discrete fracture line was visible on the left but not on the right. Follow-up radiograph performed 1 month later (Figure 3) showed healing changes at the site of the left tibial stress fracture.

Diagnosis

Stress fracture.

Differential diagnoses usually are pain related to repetitive activities or in children with a variety of conditions that result in decreased mineralization. Common repetitive activities resulting in pain in children include repeated running, jumping, throwing, or falling. Meanwhile, etiologies of decreased mineralization in children include genetically inherited osteogenesis imperfecta, rickets due to long-term vitamin D deficiency, or osteomyelitis.

Discussion

Stress fractures are microscopic cracks within bone, resulting from repetitive mechanical stress or reduced bone strength. Unlike complete fractures, stress fractures are incomplete and do not extend through the full thickness of the bone. They are broadly classified into 2 categories: fatigue fractures and insufficiency fractures. Fatigue fractures result from repeated mechanical loading that exceeds the bone's capacity for repair, commonly seen in athletes involved in repetitive high-impact activities.[1,2] In contrast, insufficiency fractures occur when normal stress is applied to weakened bone, such as in children with vitamin D deficiency or underlying metabolic bone disease.[1,3]

Figure 1. Anteroposterior radiograph of the proximal left tibia is normal.

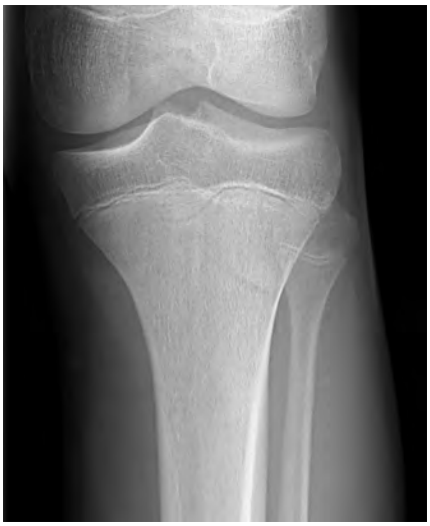

Stress fractures in children most commonly affect the lower extremities. In a retrospective analysis of pediatric lower extremity stress fractures, 28.4% were in the tibia, 24.1% in the metatarsals, 20.7% in the cuboid, 8.6% in the femur, 7.8% in the fibula, 6.9% in the calcaneus, and 3.4% in the cuneiform bones.[2] Stress fractures of the foot are frequently associated with long-distance running and high-impact sports such as basketball and soccer.[4] The

Affiliations: University of Arizona College of Medicine, Phoenix, Arizona (Ly); Department of Radiology, Phoenix Children's Hospital, Phoenix, Arizona (RB Towbin, Schaefer); Department of Radiology, Cincinnati Children's Hospital, University of Cincinnati College of Medicine, Cincinnati, Ohio (A Towbin).

Disclosures: The authors have no conflicts of interest to disclose. None of the authors received outside funding for the production of this original manuscript and no part of this article has been previously published elsewhere.

https://doi.org/10.37549/JPCR-26-0096

Figure 2. MRI performed 5 days after the initial radiograph. (A) Coronal STIR sequence of the lower legs showing edema signal within the medial aspect of each proximal tibial metaphysis. (A) T2 hypointense fracture line (arrow) is present on the left. The periosteum (arrowhead) is uplifted at the site of stress fracture. (B) Coronal T1-weighted image of the proximal left tibia showing amorphous low signal in the proximal tibia metaphysis. The periosteum (arrowhead) is uplifted at this location.

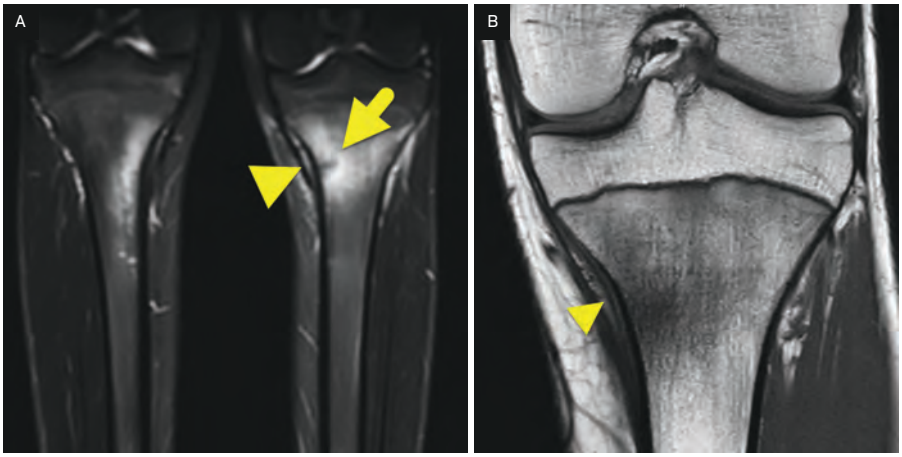

Figure 3. (A) Anteroposterior and (B) lateral radiographs performed 1 month later showing healing changes at the site of stress fracture with a linear band of sclerosis (arrow) and a healing periosteal reaction.

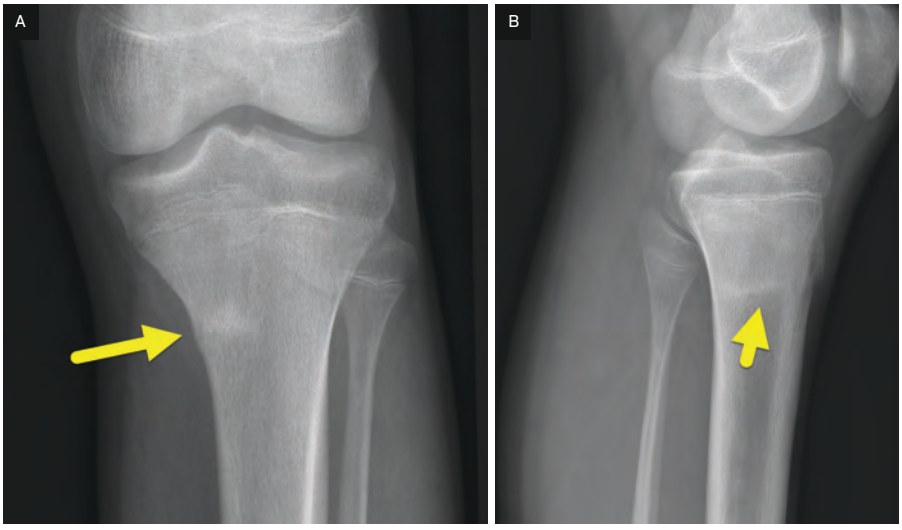

metatarsals are particularly vulnerable because they bear significant stress during the push-off phase of running.[4] Similarly, the tibia, fibula, and femur, as major weight-bearing bones, are at increased risk in children participating in high-impact activities like running and jumping.[4]

Although less common, stress fractures can also occur in the upper extremities. Examples include "little leaguer's shoulder," which involves the proximal humeral physis due to repetitive overhead throwing, and "gymnast's wrist," which affects the radial and/or ulnar physis from repetitive loading.[5] Additionally, stress fractures have been reported in the posterior column of the spine in young athletes performing repetitive spinning movements, such as figure skaters.[6]

On physical examination, stress fractures typically present with localized pain and guarding at the site of injury.[7] Because stress fractures do not cause displacement or angulation of the affected bone, skeletal deformity is not seen. Pain usually worsens with activity and improves with rest.[2] Soft tissue swelling near the fracture site may also be present.

Stress fractures can be challenging to diagnose radiographically, as fracture lines may not become visible until approximately 2 weeks after injury. Early radiographs have a sensitivity of only 15-35%, whereas MRI approaches nearly 100% sensitivity for detecting early-stage stress fractures.[1] When present, key radiographic findings include subtle lucency at the fracture site, trabecular blurring, and linear sclerosis.[1]

Advanced imaging techniques such as bone scintigraphy and MRI can improve early detection. A technetium-99m MDP bone scan can identify osseous injury 1-2 weeks earlier than radiographs.[8] On bone scintigraphy, areas of increased cortical uptake appear as hot spots, indicating osseous remodeling.[8] MRI findings include periosteal or adjacent soft tissue edema and band-like bone marrow edema.[1,3] A fracture line, when visible, appears as a hypointense band on T1-weighted sequences.[1]

The Fredericson grading system can be used to classify the severity of stress fractures on MRI, although the grading does not correlate with recovery time and is primarily used for documentation purposes.[9] The system ranges from grade 0 to grade 4b, as follows:

- **Grade 0**: normal.
- **Grade 1**: periosteal edema only, no bone marrow involvement.
- **Grade 2**: periosteal edema with bone marrow edema on T2-weighted imaging.
- **Grade 3**: periosteal edema with bone marrow edema visible on both T1- and T2-weighted imaging.
- **Grade 4a**: multiple focal intracortical signal abnormalities with bone marrow edema on T1 and T2.
- **Grade 4b**: linear intracortical signal abnormality with bone marrow edema on T1 and T2.

Because stress fractures are incomplete and cause minimal displacement, initial management is typically conservative. Treatment includes activity modification, rest, and physical therapy focused on stretching and strengthening the surrounding muscles.[7,10] If needed, immobilization with a cast for 3-6 weeks can be considered.[7] Surgical fixation with intramedullary nails or screws is reserved for high-risk fractures that may progress to complete fractures.[2]

Healing usually takes about 6-8 weeks, though recovery time varies depending on fracture location and treatment approach. Stress fractures in cortical-rich regions, such as long bone shafts, tend to heal faster than those in trabecular-rich areas, such as the epiphyseal ends.[3] Recovery time is typically longer when surgical intervention is required.[2] In one study, pediatric patients returned to activity at an average of 11.4 weeks, with recovery times ranging from 4.5 to 17.4 weeks.[2]

Conclusion

Stress fractures are microscopic disruptions of bone integrity that can occur in both children and adults. In pediatric patients, these injuries most commonly affect the lower extremities, particularly the tibia and metatarsals. Children involved in high-impact, running-intensive sports are at increased risk. Diagnosis can be challenging, as the microscopic nature of stress fractures makes them difficult to detect on radiographs. Advanced imaging modalities such as MRI and bone scintigraphy offer greater sensitivity for early detection. Because stress fractures typically do not result in displacement, treatment is generally conservative and includes activity modification, rest, and, in some cases, immobilization.

References

1) Marshall RA, Mandell JC, Weaver MJ, et al. Imaging features and management of stress, atypical, and pathologic fractures. *Radiographics*. 2018;38(7):2173-2192. doi:10.1148/rg.2018180073

2) Gremillion MJ, Martinez A, Ghanta RB, Borici N, Kushare I. An assessment of the diagnosis, treatment, and outcomes of lower extremity stress fractures in pediatric and adolescent populations. *Phys Sportsmed*. 2023;51(6):572-581. doi:10.1080/00913847.2022.2143247

3) Armento A, Heronemus M, Truong D, Swanson C. Bone health in young athletes: a narrative review of the recent literature. *Curr Osteoporos Rep*. 2023;21(4):447-458. doi:10.1007/s11914-023-00796-5

4) Strassberg J, Ahmed A. Pediatric sports injuries. *Clin Podiatr Med Surg*. 2022;39(1):89-103. doi:10.1016/j.cpm.2021.08.003

5) Kim HHR, Menashe SJ, Ngo A-V, et al. Uniquely pediatric upper extremity injuries. *Clin Imaging*. 2021;80:249-261. doi:10.1016/j.clinimag.2021.07.010

6) Kowalczyk AD, Geminiani ET, Dahlberg BW, Micheli LJ, Sugimoto D. Pediatric and adolescent figure skating injuries: a 15-year retrospective review. *Clin J Sport Med*. 2021;31(3):295-303. doi:10.1097/JSM.0000000000000743

7) Grossman J, Giliberti B, Dolitsky R, et al. Pediatric orthopedic trauma. *Pediatr Clin North Am*. 2020;67(1):101-118. doi:10.1016/j.pcl.2019.09.010

8) Serino J, Kunze KN, Jacobsen SK, et al. Nuclear medicine for the orthopedic foot and ankle surgeon. *Foot Ankle Int*. 2020;41(5):612-623. doi:10.1177/1071100720910422

9) Ditmars FS, Ruess L, Young CM, et al. MRI of tibial stress fractures: relationship between fredericson classification and time to recovery in pediatric athletes. *Pediatr Radiol*. 2020;50(12):1735-1741. doi:10.1007/s00247-020-04760-8

10) Farrell C, Hannon M, Monuteaux MC, Mannix R, Lee LK. Pediatric fracture epidemiology and US emergency department resource utilization. *Pediatr Emerg Care*. 2022;38(7):e1342-e1347. doi:10.1097/PEC.0000000000002752

Schizencephaly

Alyssa H. Sze, MS; Richard B. Towbin, MD; Carrie M. Schaefer, MD; Alexander J. Towbin, MD

Abstract

Schizencephaly is a rare cortical malformation characterized by a full-thickness gray matter-lined cleft extending from the pial surface to the ventricular wall. This defect is frequently associated with other intracranial abnormalities, including absence of the septum pellucidum, optic nerve hypoplasia, corpus callosum dysplasia, hydrocephalus, arachnoid cysts, and cerebellar malformations. While increasingly diagnosed antenatally, many patients present later in life with seizures, intellectual disability, or psychomotor delay. Clinical severity is closely related to the size and location of the cleft. Management is symptom-based and may include medical treatment for seizures, shunt placement for hydrocephalus, and supportive therapies for developmental and motor impairments.

Keywords: brain, congenital, genetic

Case Summary

An adolescent, who was a restrained passenger in a motor vehicle collision, presented to the emergency department following a brief loss of consciousness. On examination, her Glasgow Coma Scale score was 15. Notably, the patient did not have a history of seizures.

Imaging Findings

Initial head CT (Figure 1) showed no traumatic findings. Instead, the study showed the absence of the septum pellucidum, closed-lip schizencephaly in the inferior right frontal lobe with mild distortion of the adjacent lateral ventricle, and closed-lip schizencephaly and polymicrogyria in the left frontal lobe. Subsequent MRI (Figure 2) confirmed these findings.

Figure 1. Axial CT images at the level of (A) the frontal horns of the lateral ventricles and (B) the body of the lateral ventricles showing the absence of the septum pellucidum and bilateral closed-lip schizencephaly (arrow) with gray matter lining each cleft.

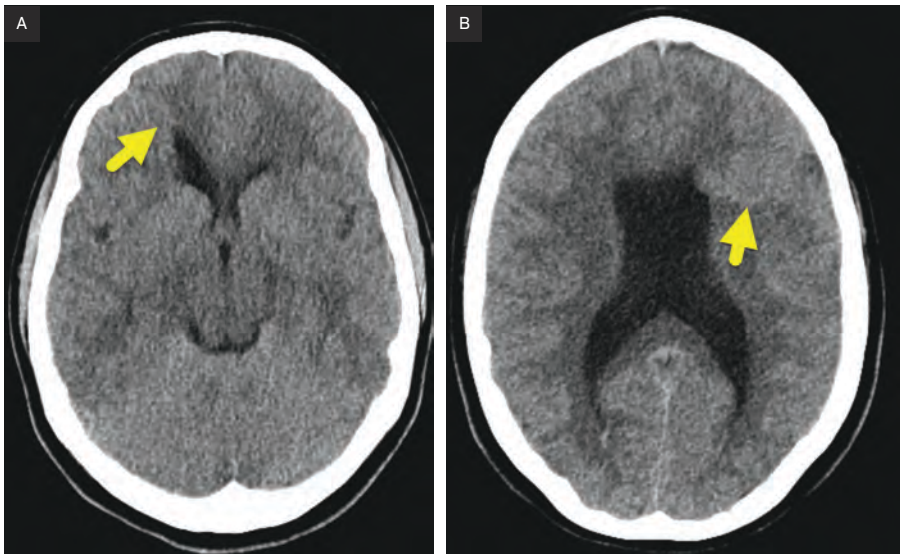

Diagnosis

Schizencephaly.

The imaging differential diagnosis for schizencephaly includes porencephaly, heterotopic gray matter, gliosis, focal cortical dysplasia, polymicroglia, arachnoid cysts, and septo-optic dysplasia.

Discussion

Schizencephaly is a rare malformation of the cerebral cortex occurring with a prevalence of 1.54 per 100,000

Affiliations: Virginia Tech Carilion School of Medicine, Roanoke, Virginia (Sze); Department of Radiology, Phoenix Children's Hospital, Phoenix, Arizona (RB Towbin, Schaefer); Department of Radiology, Cincinnati Children's Hospital, University of Cincinnati College of Medicine, Cincinnati, Ohio (AJ Towbin).
Disclosures: The authors have no conflicts of interest to disclose. None of the authors received outside funding for the production of this original manuscript and no part of this article has been previously published elsewhere.

https://doi.org/10.37549/JPCR-26-0097

Figure 2. (A) Axial T2-weighted and (B) T1 FLAIR images at the level of the frontal horns of the lateral ventricles and (C) axial T2-weighted and (D) T1 FLAIR images at the level of the mid body of the lateral ventricles showing the absence of the septum pellucidum and bilateral closed-lip schizencephaly (arrow) with gray matter lining each cleft. Polymicrogyria is present at each cleft.

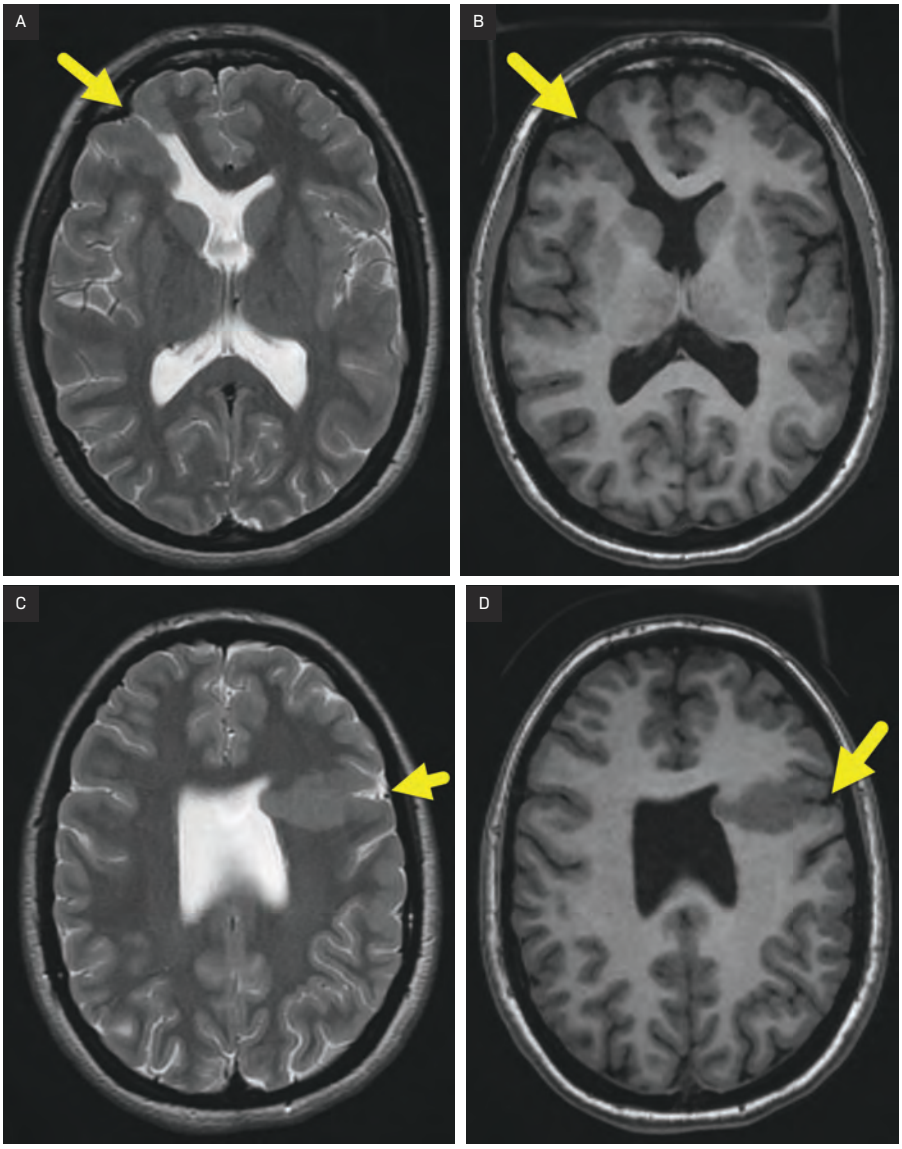

births.[1] It is characterized by a full-thickness gray matter-lined cleft that extends from the pial surface to the ventricular wall. The cleft's gray matter lining distinguishes it from other cortical abnormalities.[2] Schizencephaly typically occurs sporadically. Only a few familial cases have been described.[3] However, it has been occasionally associated with mutations in the *EMX2* and *COL4A1* genes, as well as with Vici syndrome, a disorder caused by *EPG5* gene mutations and characterized by agenesis of the corpus callosum, cardiomyopathy, albinism, and immune deficiency.

The etiology of schizencephaly remains unclear. Proposed mechanisms include intrauterine infections and early vascular disruptions.[1] One hypothesis suggests that intracranial insults occurring before neuronal migration (4-6 months gestational age) result in schizencephaly, while injuries after this period produce defects not lined by gray matter, such as porencephaly (without gliosis) or encephalomalacia (with gliosis).[4] Additional risk factors include young maternal age (under 20 years), prenatal exposure to toxins or teratogens, and maternal trauma.[3]

Schizencephaly can be distinguished from other intracranial abnormalities, such as porencephaly, by the presence of a gray matter lining along the cleft. Porencephaly refers to a cystic cavity within the cerebral hemisphere that communicates with the ventricular system or subarachnoid space. These cavities are typically surrounded by gliosis, lack a gray matter lining, and are usually the result of acquired brain injury. While antenatal US is increasingly capable of detecting schizencephaly in utero, MRI remains the preferred imaging modality due to its ability to clearly visualize the gray matter lining.[3]

Schizencephaly is typically classified into 2 types: type 1 (closed-lip) and type 2 (open-lip). In open-lip schizencephaly, the cleft walls are separated and filled with cerebrospinal fluid. In contrast, closed-lip schizencephaly is characterized by direct apposition of the cleft walls without intervening fluid. More recent literature proposes an expanded classification that includes a third variant: a column of heterotopic gray matter without a visible cleft. In this system, type 1 represents isolated gray matter heterotopia, type 2 corresponds to closed-lip schizencephaly, and type 3 to open-lip schizencephaly.[1,4]

Open-lip schizencephaly is the most common form, seen in approximately 80-85% of patients, while closed-lip accounts for the remaining 10-15%. Schizencephaly may be unilateral or bilateral, with bilateral involvement slightly more frequent. Among patients with bilateral clefts, 60% have bilateral open-lip defects, and 20% have mixed defects. Of those with unilateral clefts, 60% have open-lip defects.[4]

Between 50% and 90% of patients with schizencephaly have additional intracranial anomalies. The most common

associated abnormality is absence of the septum pellucidum, seen in approximately 70% of patients. Other frequent findings include optic nerve hypoplasia (30%), corpus callosum dysplasia (30%), and hydrocephalus, which occurs in about 30% of patients with open-lip clefts.[3-5] Additional associations include arachnoid cysts and cerebellar malformations.[3]

When schizencephaly is not detected on antenatal imaging, it is often identified later in childhood during evaluation for psychomotor delay or seizures. In patients with a unilateral cleft, seizures may originate from the contralateral hemisphere, often in regions of polymicrogyria.[5] The severity of symptoms and overall prognosis correlates with the size and location of the cleft. Larger or bilateral defects are associated with more significant motor and cognitive impairments, including hemiparesis or quadriparesis, intellectual disability, language deficits, and global developmental delay.[1,6] Frontal or perisylvian clefts may also be associated with behavioral disturbances or characteropathies.[3]

In contrast, unilateral schizencephaly may be asymptomatic and is sometimes discovered incidentally in adulthood, often after the onset of seizures in individuals with otherwise normal development.[7] Treatment is symptom-directed and may include antiepileptic medications, ventriculoperitoneal shunting for hydrocephalus, and supportive therapies such as occupational and physical therapy to address cognitive and motor impairments.[1,8]

Conclusion

Schizencephaly is a rare cortical malformation characterized by a full-thickness gray matter-lined cleft extending from the pial surface to the ventricular wall. This defect is frequently associated with other intracranial abnormalities, including the absence of the septum pellucidum, optic nerve hypoplasia, corpus callosum dysplasia, hydrocephalus, arachnoid cysts, and cerebellar malformations. While increasingly diagnosed antenatally, many patients present later in life with seizures, intellectual disability, or psychomotor delay. Clinical severity is closely related to the size and location of the cleft. Management is symptom-based and may include medical treatment for seizures, shunt placement for hydrocephalus, and supportive therapies for developmental and motor impairments.

References

1) Hashim HT, Ahmad MS, Gataa IS. Schizencephaly. In: AlAli KF, Hashim HT, eds. *Congenital Brain Malformations*. Springer. 2024. doi:10.1007/978-3-031-58630-9_14

2) Oh KY, Kennedy AM, Frias AE Jr, Byrne JLB. Fetal schizencephaly: pre- and postnatal imaging with a review of the clinical manifestations. *Radiographics*. 2005;25(3):647-657. doi:10.1148/rg.253045103

3) Halabuda A, Klasa L, Kwiatkowski S, et al. Schizencephaly-diagnostics and clinical dilemmas. *Childs Nerv Syst*. 2015;31(4):551-556. doi:10.1007/s00381-015-2638-1

4) Griffiths PD. Schizencephaly revisited. *Neuroradiology*. 2018;60(9):945-960. doi:10.1007/s00234-018-2056-7

5) Naidich TP, Griffiths PD, Rosenbloom L. Central nervous system injury in utero: selected entities. *Pediatr Radiol*. 2015;45(s3):S454-62. doi:10.1007/s00247-015-3344-6

6) Hung P-C, Wang H-S, Chou M-L, et al. Schizencephaly in children: a single medical center retrospective study. *Pediatr Neonatol*. 2018;59(6):573-580. doi:10.1016/j.pedneo.2018.01.009

7) Paudel K, Prasad T, Gyawali P, Nepal G, Jaiswal V. Schizencephaly diagnosed after an episode of seizure during labor: a case report. *Clin Case Rep*. 2023;11(5):e7328. doi:10.1002/ccr3.7328

8) Ghosn Y, Kamareddine MH, Adem C, Jabbour R. A patient with schizencephaly and agenesis of corpus callosum with no neurological deficits. *J Neurosci Rural Pract*. 2018;9(3):404-405. doi:10.4103/jnrp.jnrp_564_17

Lymphangioleiomyomatosis

Tal A. Chamdi, BS; Richard B. Towbin, MD; Carrie M. Schaefer, MD; Alexander J. Towbin, MD

Abstract

Although the diagnosis of tuberous sclerosis complex-lymphangioleiomyomatosis (TSC-LAM) is rare in adolescents, emerging data suggest that its true incidence, particularly among females with TSC, may be underestimated. High-resolution CT of the chest is critical for identifying characteristic pulmonary cysts, while abdominal imaging plays a supportive role by detecting associated renal angiomyolipomas. Given the progressive nature of LAM, early recognition is essential for guiding management and improving outcomes. Clinicians should maintain a high index of suspicion for LAM in adolescents with TSC2 gene mutations.

Keywords: pulmonary, lung, congenital

Case Summary

An adolescent female with tuberous sclerosis complex (TSC) underwent screening chest CT.

Imaging Findings

Initial chest CT (Figure 1) demonstrated multiple small, thin-walled cysts predominantly located in the right lower lobe, consistent with early findings of lymphangioleiomyomatosis (LAM). Follow-up chest CT (Figure 2) performed 12 years later showed mild progression in the number and size of pulmonary cysts. Abdominal MRI (Figure 3) revealed multiple renal angiomyolipomas (AMLs), most of which were lipid-poor. The largest lesion was in the lower pole of the right kidney.

Diagnosis

TSC-LAM.

Differential diagnosis includes sporadic LAM, emphysema, Sjögren syndrome, pulmonary Langerhans cell histiocytosis, follicular bronchiolitis, lymphoid interstitial pneumonia, amyloidosis, light-chain deposition disease, and Birt-Hogg-Dube syndrome.

Discussion

LAM is a rare, progressive multisystem disease that primarily affects women of childbearing age, with an estimated prevalence of 3.4-7.8 per million women worldwide.[1] It is characterized by the proliferation of abnormal smooth muscle—like cells that infiltrate the lungs and lymphatics, leading to progressive cystic destruction, impaired pulmonary function, and, ultimately, respiratory failure.[2]

LAM occurs in 2 forms: a sporadic form, which typically presents in adulthood, and a form associated with TSC, which may present in childhood.[2] TSC-LAM is increasingly recognized as a significant cause of morbidity in women with TSC. Among adult women with TSC, approximately 30-40% will develop LAM. The condition is significantly more common in those with TSC2 mutations than in those with TSC1 mutations, with one study reporting a prevalence of 55% vs 0%, respectively.[3] Serum VEGF-D levels are also typically higher in patients with LAM and TSC2 mutations and may serve as a useful biomarker for the presence of LAM.[3] In a study by Cudzilo et al, the prevalence of LAM in females under the age of 21 with TSC was 27%, suggesting that disease onset may occur earlier than previously recognized.[4] Another study showed that lung cysts were present in 12% of patients with TSC who had received a chest CT, including 20% of women.[5] Nevertheless, diagnosis in adolescents remains rare, likely due to a combination of factors, including the absence of respiratory symptoms, lack of universal screening protocols in the pediatric populations, and the subtle, nonspecific appearance of early pulmonary changes on imaging.[4,6]

In adolescents, TSC-LAM is often asymptomatic, but when symptoms do occur, they may include exertional dyspnea or spontaneous pneumothorax. Imaging, chest CT, plays a central role in diagnosis. According to the 2017 American Thoracic Society/Japanese Respiratory Society guidelines, LAM can be diagnosed

Affiliations: Central Michigan University, College of Medicine, Mount Pleasant, Michigan (Chamdi); Phoenix Children's Hospital, Phoenix, Arizona (RB Towbin, Schaefer); Cincinnati Children's Hospital, Cincinnati College of Medicine, Cincinnati, Ohio (AJ Towbin).
Disclosures: The authors have no conflicts of interest to disclose. None of the authors received outside funding for the production of this original manuscript and no part of this article has been previously published elsewhere.

https://doi.org/10.37549/JPCR-26-0098

Figure 1. (A, B) Sequential images from chest CT showing several small cysts (arrows) with imperceptible walls.

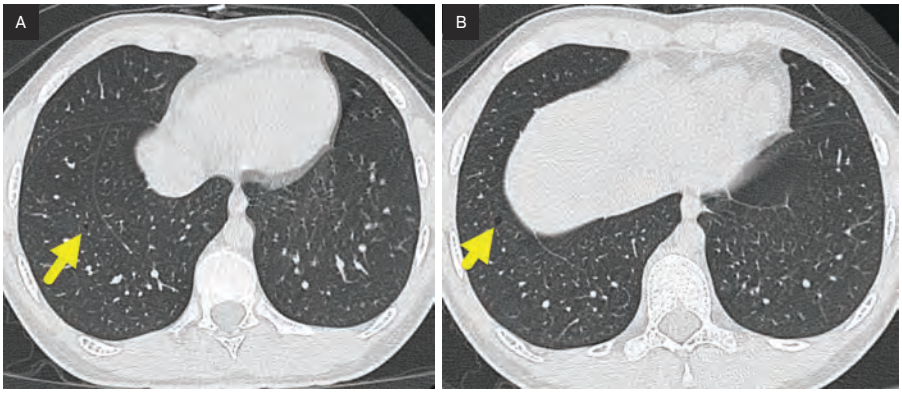

Figure 2. (A, B) Sequential images from chest CT performed 12 years later showing that the small cysts (arrow) have increased in size and number. (C, D) Minimum intensity projection images at the same levels highlighting the extent of the small cysts.

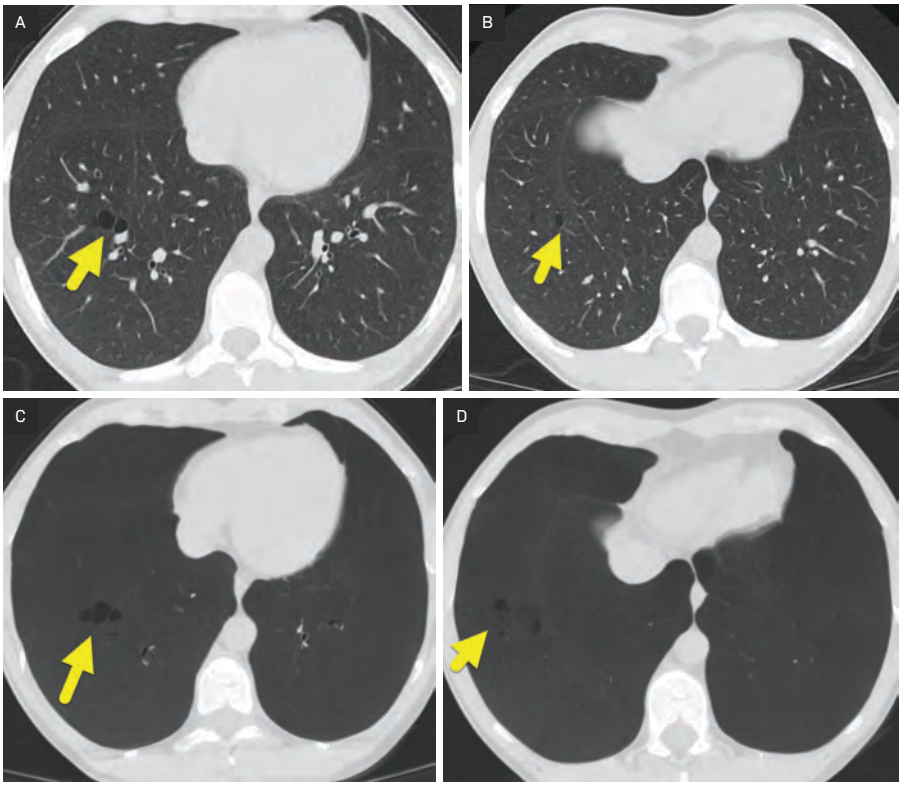

based on the presence of characteristic diffuse, thin-walled, round pulmonary cysts, in conjunction with one or more supportive features, such as TSC, renal AML, cystic lymphangioleiomyoma, chylothorax, or chylous ascites.[7]

Chest radiographic findings vary depending on disease severity: patients with early-stage disease may have a normal radiograph or may have mildly increased interstitial markings. Patients with advanced disease may demonstrate reticular opacities, pleural thickening, lymphadenopathy, and hyperinflation.[1,2]

Current TSC guidelines recommend baseline chest CT for all females and symptomatic males, starting at 18 years of age.[8] On chest CT, TSC-LAM is characterized by numerous thin-walled, round, or oval cysts distributed throughout the

Figure 3. Coronal T2-weighted MRI showing a dominant lipid-poor angiomyolipoma in the lower pole of the right kidney. There are many tiny angiomyolipomata throughout both kidneys, giving the cortex a striated appearance.

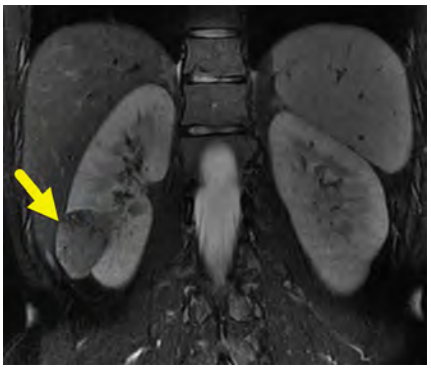

lungs.[1] In early disease, cysts are fewer and smaller, with intervening normal lung parenchyma. At this stage, the cysts may be more visible on minimum intensity projection images. As the disease progresses, cysts become more numerous and larger, gradually replacing healthy lung tissue. Additional CT findings may include focal ground-glass opacities, lymphatic congestion, septal thickening, chylothorax, pericardial effusion, and thoracic duct dilation.[1,2] TSC-LAM may also be associated with multifocal micronodular pneumocyte hyperplasia.[1] Certain imaging features help distinguish LAM from other diffuse cystic lung diseases. For example, thick, irregular upper lobe cysts are more typical of pulmonary Langerhans cell histiocytosis.[1]

Abdominal and pelvic imaging with CT or MRI is essential, as over 90% of patients with TSC-LAM and approximately one-third of those with sporadic LAM have renal AMLs.[9] On CT, AMLs typically involve the renal cortex and often contain macroscopic fat. However, in patients with TSC-LAM, up to one-third of AMLs may be fat-poor, making detection more challenging.[10] On MRI, classic AMLs demonstrate signal loss on fat-suppressed sequences. Chemical shift MRI can also detect small amounts of fat by revealing signal loss within voxels that contain both fat and water, often

producing an "India-ink" artifact at the fat-water interface of the lesion.[11]

Management of LAM focuses on alleviating symptoms and slowing disease progression. Recurrent or complicated pneumothoraces may be treated with pleurodesis, and lung transplantation is considered in patients with advanced respiratory failure. More recently, mTOR inhibitors such as sirolimus have emerged as a key therapy, shown to stabilize lung function and reduce the size of associated tumors in patients with LAM.[1,2]

Conclusion

Although the diagnosis of TSC-LAM is rare in adolescents, emerging data suggest that its true incidence, particularly among females with TSC, may be underestimated. High-resolution CT of the chest is critical for identifying characteristic pulmonary cysts, while abdominal imaging plays a supportive role by detecting associated renal AMLs. Given the progressive nature of LAM, early recognition is essential for guiding management and improving outcomes. Clinicians should maintain a high index of suspicion for LAM in adolescents with TSC2 gene mutations.

References

1) McCarthy C, Gupta N, Johnson SR, Yu JJ, McCormack FX. Lymphangioleiomyomatosis: pathogenesis, clinical features, diagnosis, and management. *Lancet Respir Med*. 2021;9(11):1313-1327. doi:10.1016/S2213-2600(21)00228-9

2) O'Mahony AM, Lynn E, Murphy DJ, Fabre A, McCarthy C. Lymphangioleiomyomatosis: a clinical review. *Breathe*. 2020;16(2):200007. doi:10.1183/20734735.0007-2020

3) Tian X, Glass JE, Kwiatkowski DJ, et al. Lymphangioleiomyomatosis association with underlying genotype in patients with tuberous sclerosis complex. *Ann Am Thorac Soc*. 2021;18(5):815-819. doi:10.1513/AnnalsATS.202008-911OC

4) Cudzilo CJ, Szczesniak RD, Brody AS, et al. Lymphangioleiomyomatosis screening in women with tuberous sclerosis. *Chest*. 2013;144(2):578-585. doi:10.1378/chest.12-2813

5) Ritter DM, Fessler BK, Ebrahimi-Fakhari D, et al. Prevalence of thoracoabdominal imaging findings in tuberous sclerosis complex. *Orphanet J Rare Dis*. 2022;17(1):124. doi:10.1186/s13023-022-02277-x

6) Johnson J, Somerfield W, Johnson SR. Lymphangioleiomyomatosis in patients with tuberous sclerosis: a national centre audit. *Orphanet J Rare Dis*. 2024;19(1):137. doi:10.1186/s13023-024-03115-y

7) McCormack FX, Gupta N, Finlay GR, et al. Official American thoracic society/Japanese respiratory society clinical practice guidelines: lymphangioleiomyomatosis diagnosis and management. *Am J Respir Crit Care Med*. 2016;194(6):748-761. doi:10.1164/rccm.201607-1384TH

8) Northrup H, Aronow ME, Bebin EM, et al. Updated international tuberous sclerosis complex diagnostic criteria and surveillance and management recommendations. *Pediatr Neurol*. 2021;123:50-66. doi:10.1016/j.pediatrneurol.2021.07.011

9) Avila NA, Dwyer AJ, Rabel A, Moss J. Sporadic lymphangioleiomyomatosis and tuberous sclerosis complex with lymphangioleiomyomatosis: comparison of CT features. *Radiology*. 2007;242(1):277-285. doi:10.1148/radiol.2421051767

10) Silverman SG, Israel GM, Herts BR, Richie JP. Management of the incidental renal mass. *Radiology*. 2008;249(1):16-31. doi:10.1148/radiol.2491070783

11) Thiravit S, Teerasamit W, Thiravit P. The different faces of renal angiomyolipomas on radiologic imaging: a pictorial review. *Br J Radiol*. 2018;91(1084):20170533. doi:10.1259/bjr.20170533

Double Aortic Arch Case

Naim S. Duran, BS; Lydia M. Pastore, BS; Richard B. Towbin, MD; Jason N. Johnson, MD,MHS; Ranjit Philip, MD; Alexander J. Towbin, MD

Abstract

Double aortic arch is a congenital vascular anomaly of the primitive aortic arches that leads to compression of the trachea and/or the esophagus. Children with a double aortic arch usually present with nonspecific signs of tracheal/esophageal compression such as dysphagia, cough, respiratory failure, and choking. Consequently, vascular rings such as the double aortic arch are often found incidentally on imaging and may be further evaluated using transthoracic echocardiography, MR angiography, or CTA. Management of symptomatic cases of double aortic arch involves surgical repair in which the nondominant branch is resected, leading to an excellent prognosis and survival.

Keywords: cardiothorcic, cardiac, congenital

Case Summary

A toddler presented with noisy breathing and intermittent stridor over the last few months associated with feeding difficulties. On physical examination, the patient had inspiratory stridor at rest with mild subcostal retractions and intermittent wheezing, while the cardiovascular exam was unremarkable with normal heart sounds.

Imaging Findings

Chest CT with contrast (Figures 1-4) showed a double aortic arch (DAA) with the same-size left and right aortic arches. There was narrowing of the distal trachea and mid esophagus (Figures 3, 4) at the level of the DAA.

Diagnosis

Double aortic arch.

Differential diagnostic considerations based on the clinical findings are tracheomalacia, laryngomalacia, laryngeal web, laryngeal cyst, mediastinal mass (lymphoma), tracheoesophageal fistula, asthma, gastroesophageal reflux disease, bronchiolitis, and recurrent lower respiratory tract infection. Imaging-based differential diagnosis includes a right aortic arch with an aberrant left subclavian artery, pulmonary artery sling, brachiocephalic artery compression, and mediastinal masses.

Discussion

Vascular rings are congenital abnormalities of the embryological aortic vessels, which may surround the trachea and/or the esophagus and lead to compression of adjacent structures. These vascular ring anomalies have been described as early as 1737 by Hommel, with descriptions of tracheal and esophageal obstruction being described in 1837 by von Siebold.[1] Development of the aortic arch occurs between weeks 2 and 7 of gestation, during which 6 pairs of primitive aortic arches form, and certain arches involute to form the normal left-sided aortic arch. Arches 1 and 2 regress, leaving the hyoid, maxillary, and stapedial arteries, while

Figure 1. Chest CT with contrast in an axial plane. There is a double aortic arch with co-dominant arches encircling the trachea and esophagus. LAA, left aortic arch; RAA, right aortic arch.

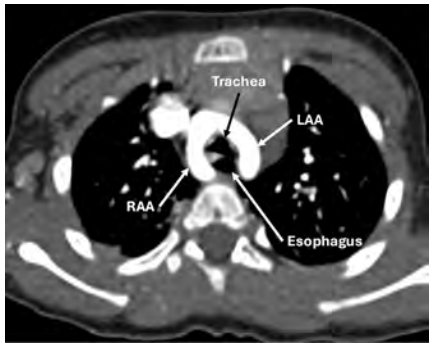

Affiliations: University of Arizona College of Medicine, Phoenix, Arizona (Duran, Pastore); Department of Radiology, Phoenix Children's Hospital, Phoenix, Arizona (RB Towbin); Heart Institute, Le Bonheur Children's Hospital, Memphis, Tennessee (Johnson, Philip); Department of Radiology, Cincinnati Children's Hospital, University of Cincinnati College of Medicine, Cincinnati, Ohio (A Towbin).

Disclosures: The authors have no conflicts of interest to disclose. None of the authors received outside funding for the production of this original manuscript and no part of this article has been previously published elsewhere.

https://doi.org/10.37549/JPCR-26-0095

Figure 2. Chest CT with contrast 3D reconstruction off-axis coronal projection from posterior. There is a double aortic arch with co-dominant arches. The right subclavian and right common carotid arteries arise from the right aortic arch. The left subclavian and left common carotid arteries arise from the left aortic arch. DA, descending aorta; LAA, left aortic arch; LCCA, left common carotid artery; LPA, left pulmonary artery; LSA, left subclavian artery; RAA, right aortic arch; RCCA, right common carotid artery; RPA, right pulmonary artery; RSA, right subclavian artery.

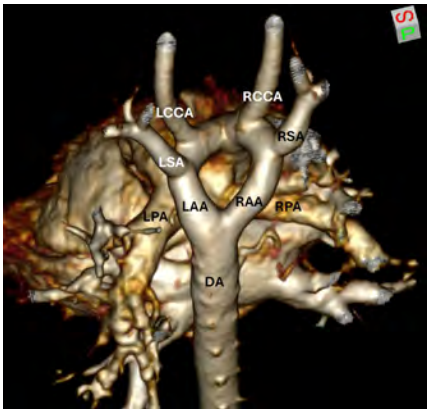

Figure 3. Chest CT with contrast dynamic airway assessment coronal projection. There is distal tracheal narrowing (arrow) at the left of the double aortic arch.

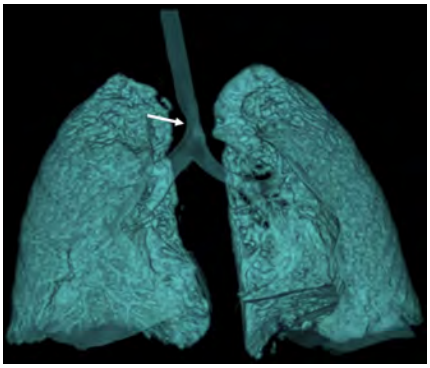

Figure 4. (A) Chest CT with contrast hollow vessel 3D reconstruction off-axis coronal projection from posterior. There is a double aortic arch with co-dominant arches with compression of the distal trachea (arrow) and mid esophagus. DA, descending aorta; LAA, left aortic arch; LB, left bronchus; LCCA, left common carotid artery; LE, lower esophagus; LSA, left subclavian artery; RAA, right aortic arch; RB, right bronchus; RCCA, right common carotid artery; RSA, right subclavian artery; T, trachea; UE, upper esophagus. (B). Chest CT with contrast hollow vessel 3D reconstruction sagittal projection. There is compression of the mid esophagus (asterisk) and narrowing of the distal trachea (arrow) at the level of the double aortic arch. DA, descending aorta; LAA, left aortic arch; LB, left bronchus; LCCA, left common carotid artery; LE, lower esophagus; LSA, left subclavian artery; RAA, right aortic arch; T, trachea; UE, upper esophagus.

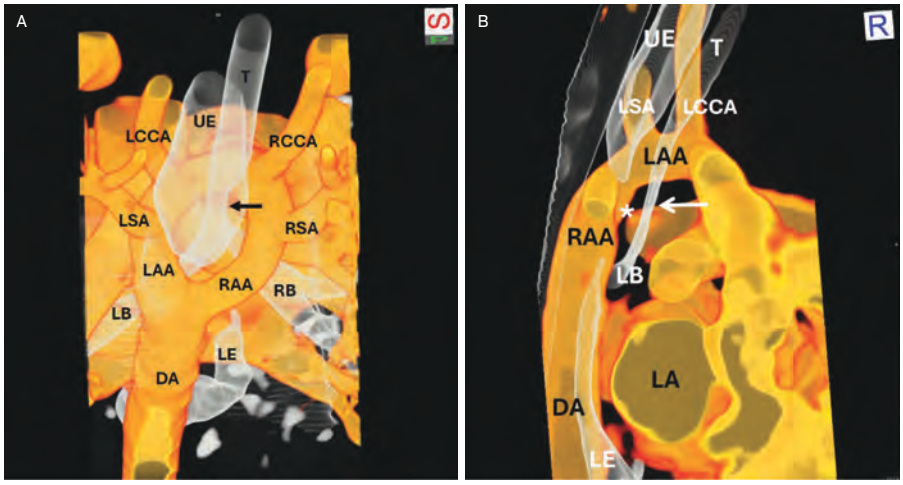

arch 3 forms the common carotid and part of the internal carotid arteries. The 4th pair of aortic arches forms bilateral aortic arches, after which the right-sided arch regresses in week 5 of gestation, with the left-sided aortic arch remaining.[2]

While multiple variants of vascular rings exist with complete, partial, or atretic segments, the most common is the DAA in which there is complete encirclement of the esophagus and trachea. There are 3 main types of DAA: left dominant, right dominant, and co-dominant arch. The true incidence of the DAA is not well established; however, data from a 20-year single-center study found the incidence of all aortic arch anomalies to be 0.033% and all ring-forming anomalies to be 0.021%.[3] In children with DAA, the median maternal age was higher, the incidence of conceptions from in vitro fertilization was higher, and the incidence of DAA in 22q11 deletions was 14%.[4,5]

As the anatomy of DAA anomalies may have multiple variations, the presentation depends on the degree of compression of the trachea and esophagus. Presenting symptoms can range from acute manifestations of tracheal/esophageal compression to subtle subacute signs. In general, esophageal compression in children with DAA may present with persistent dysphagia, choking, regurgitation, and potentially failure to thrive. With respect to tracheal compression, children may present with acute signs of respiratory failure, cyanosis, and apneic episodes, or more subtle signs such as wheezing, stridor, persistent cough, and recurring lower respiratory tract infections.[2] Findings on physical exam and laboratory tests are generally nonspecific but may be helpful in ruling out other potential causes.

Echocardiography, cardiac MRI, CTA, and barium esophagrams may all be useful in the diagnosis of vascular rings. Transthoracic echocardiography may be the initial imaging modality used due to it being minimally invasive and the lack of radiation exposure. On the other hand, the complexity of certain vascular anomalies will likely require MR angiography or CTA for adequate visualization, especially in the presence of life-threatening sequelae.[6] The disadvantage of MR angiography is the longer acquisition times likely requiring sedation of pediatric patients, while for CTA, it is the pediatric exposure to radiation. Many with DAA go undiagnosed or may incidentally be found during various forms of imaging. Vascular rings may be found incidentally during barium esophagram, evaluating the potential causes of dysphagia. Similarly, tracheal compression may be found incidentally during bronchoscopy for the evaluation of respiratory symptoms.

The first documented surgical repair of a vascular ring was described in 1947, and the current standard treatment

for most DAA cases remains to be surgical intervention, with the goal of releasing the compression on the trachea and/or the esophagus.[2,7] Generally, the approach is via a muscle-sparing thoracotomy on the nondominant side. The surgery involves entering the chest cavity, identifying important structures such as the vagus and phrenic nerves, occluding the nondominant arch, and lastly dividing the nondominant arch and ligamentum arteriosum.[2,5,8] In the case of a co-dominant arch, the posterior arch is resected to preserve a more anatomic structure. Surgery is largely successful (95-98%), with most patients undergoing DAA repair having good prognoses. Follow-up after surgery tends to yield relatively mild respiratory or gastrointestinal symptoms, likely related to compression-related maldevelopment.

Conclusion

DAA is a congenital vascular anomaly of the primitive aortic arches that leads to compression of the trachea and/or the esophagus. Children with a DAA usually present with nonspecific signs of tracheal/esophageal compression such as dysphagia, cough, respiratory failure, and choking. Consequently, vascular rings such as the DAA are often found incidentally on imaging and may be further evaluated using transthoracic echocardiography, MR angiography, or CTA. Management of symptomatic cases of DAA involves surgical repair in which the nondominant branch is resected, leading to an excellent prognosis and survival.

References

1) Edwards FR. Vascular compression of the trachea and oesophgus. *Thorax*. 1959;14(3):187-200. doi:10.1136/thx.14.3.187

2) Tarmahomed A, Umapathi KK. Double aortic arch. In: *StatPearls* [Internet]. StatPearls Publishing. 2021.

3) Kaldararova M, Simkova I, Varga I, et al. Double aortic arch anomalies in children: a systematic 20-year single center study. *Clin Anat*. 2017;30(7):929-939. doi:10.1002/ca.22955

4) Vigneswaran TV, Jabak S, Syngelaki A, et al. Prenatal incidence of isolated right aortic arch and double aortic arch. *J Matern Fetal Neonatal Med*. 2021;34(18):2985-2990. doi:10.1080/14767058.2019.1676413

5) Alsenaidi K, Gurofsky R, Karamlou T, Williams WG, McCrindle BW. Management and outcomes of double aortic arch in 81 patients. *Pediatrics*. 2006;118(5):e1336-41. doi:10.1542/peds.2006-1097

6) Hanneman K, Newman B, Chan F. Congenital variants and anomalies of the aortic arch. *Radiographics*. 2017;37(1):32-51. doi:10.1148/rg.2017160033

7) Gross RE. Surgical relief for tracheal obstruction from a vascular ring. *N Engl J Med*. 1945;233:586-590. doi:10.1056/nejm194511152332003

8) Backer CL, Mongé MC, Popescu AR, et al. Vascular rings. *Semin Pediatr Surg*. 2016;25(3):165-175. doi:10.1053/j.sempedsurg.2016.02.009